REACTION-DIFFUSION MODELLING: QUANTITATIVE STUDY OF GEOMETRY-ACTIVITY RELATIONSHIP OF FINNED ZEOLITE CATALYST & MODEL STUDY OF MAXWELL-STEFAN FORMUALATION WITH DIFFERENT ADSORPTION MECHANISMS

By

YILIN YANG

A thesis submitted to Johns Hopkins University in conformity with the requirements for the degree of
Master of Science in Engineering

Baltimore, Maryland

May,2021

Abstract

The improved catalytic performance of nano-sized zeolite with considerably reduced internal diffusion limitation has stimulated the research on the synthesis of new structure/geometry of catalyst for industry application. In 2020, Rimer's group developed a new finned zeolite catalyst with significant reduced internal diffusion limitation by epitaxial growth of finned like protrusion.[4] The first chapter of this thesis focusses on the simulation of the effect of geometry of this finned zeolite on selectivity and diffusion limitation. A reaction-diffusion mathematical model is built to examine the geometry-selectivity relationship via simulation of two parallel liquid phase reactions (self-etherification and alkylation). Finned catalysts with four different geometries are chosen and compared with conventional sphere catalyst of similar size.

The second chapter of this thesis is about the modelling of zeolite catalyzed reaction, adsorption, and diffusion inside the zeolite crystal via using Stefan-maxwell and Langmuir-Hinshelwood formulation. Two mostly common adsorption approach, multicomponent Langmuir isotherm (MCL) and Ideal adsorption solution theory (IAST) are applied in the model. By simulating gas n-Hexane isomerization reaction in MFI zeolite, the difference of reaction-diffusion models with IAST model and MCL model is shown. The simulation results are compared with results reference papers.[20][21]

Advisor: Dr. Michael Tsapatsis

Reader: Dr. Chao Wang

Acknowledgement

I would like to express thankfulness to my research advisor Dr.Michael Tsapatsis for his patience and thoughtful guidance in my research. During my one year's master research, Dr.Tsapatsis taught me from the very beginning stage and provided me all ability needed to be a qualified researcher. It is my honor to have Dr Tsapatsis to be my advisor.

I also want to thank Dr.Dandan Xu for her assistance on understanding of reference papers and terminologies. I want to thank Dr. Zhe Li for his spiritual encouragement and persuasion all the time.

Contents

List of Tables

List of Figures

Chapter 1

Introduction

The well-defined channel framework of zeolite has been applied to many industry applications from catalyst, adsorbent to selective separation. One of objective for zeolite design is to reduce diffusion limitation and increase accessibility of acid site via increasing mesopores and micropores, therefore enhance selectivity, activity, and reduce accumulation of coke species. Recently, Multiple literature have revealed that,[1] [2] Nano-sized zeolite crystal, like self-pillared zeolite and 2-dimensional zeolite, have shown better selectivity and longer lifetime compared to conventional zeolite. [3] Nano-sized crystal can have a few units cell thickness, with more acid site on external surface and more mesopore, which show favorable effect on mass transfer and selectivity. In 2020. Rimer's group synthesized a finned like zeolite catalyst, with rough protrusion on the external surface of nano-sized seed MFI type (ZSM-5 and ZSM-11) crystal. [4] The geometry of this new catalyst is shown in figure 1. It is reported that this new geometry catalyst has markedly reduced the diffusion path length with increasing molecular uptake rate in fin, which result in less coke formation on the external surface and high product selectivity.[4] This thesis is trying to simulate and verify the effect of the fin (protrusion) geometry on the mass transfer properties via building a reaction and diffusion model. The validity of the numerical model is verified by comparing with the analytical model. The activity of the finned catalyst will compare with activity of same size conventional spherical catalysts, which is calculated by analytical method. This model could lead to rational design of this finned catalyst.

To reveal the effect of the geometry on the performance (selectivity) of the catalyst, especially the difference between the external surface and seed crystal, two parallel test reaction, self-esterification, and alkylation reaction with mesitylene are chosen. The reaction mechanism is shown in figure 2. The benzyl

alcohol is converted to 1,3,5-trimethyl-2-benzylbenzene and benzyl ether in liquid phase. Alkylation reaction only occurs at the surface of the crystal and self-etherification reaction occur at both micropore and surface of crystal. Therefore, the selectivity of two reactions can provide a quantitative assessment of activity of external surface and internal micropores.

Figure 2 Idealized schematic of a finned zeolite and Transmission electron micrograph of a representative finned ZSM-11 crystal. *
*pictures come from literature [4]
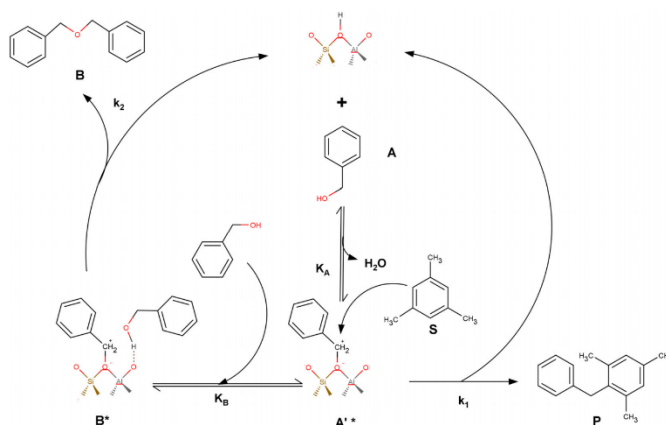
Figure 2 the mechanisms for benzyl alcohol etherification (left) and alkylation (right) reactions in liquid phase*
*Picture come from the literature.[5]

Modeling

Reaction mechanism

The reaction mechanism is shown in figure 1. A Bronsted acid site(BAS) adsorbs the benzyl alcohol and prontonate it to form a carbonium ion(A'*).The free or weakly adsorbed mestylene(S) may react with the Protonated benzyl alcohol and form 1,3,5-trimethyl-2-benzylbenzene(P). Carbonium also could react with another adsorbed benzyl alcohol(B*) to form benzyl ether. The kinetic rate expression for alkylation at the external surface is shown as equation 1, which is derived in literature [5], assumes that all adsorbed steps are quasi-equilibrium equation. Protonated benzyl alcohol(A'*). and co-adsorbed benzyl alcohol (B*) are the dominant surface species.

$$r_P = \frac{dC_P}{dt} = \frac{k_{1s}}{1+K_B C_A} C_{H^+} f_{ext} \hspace{3cm} \text{Equation 1}$$

C_p represent the concentration of 1,3,5-trimethyl-2-benzylbenzene. C_A is the concentration of benzyl alcohol. K_B denote the equilibrium constant for formation of co-adsorbed benzyl alcohol. K_{1s} represents effective alkylation rate constant related to reaction. C_{H^+} is the concentration of BAS in catalyst. Since the Si/Al ratio of finned MFI catalyst made by seeded analysis =32.6, which is close to the ratio of 0.2 μm MFI synthesized by Dandan.et.al (Si/Al=33), therefore we assume the BAS density of finned MFI catalyst is equal to that of 0.2 μm MFI, which is $489 \frac{\mu mol}{g}$. BAS concentration C_{H^+}=BAS density×weight of catalyst/volume of reactor, where weight of catalyst is 0.025g. and volume of reactor is15.25mL.

f_{ext} is the external acid site fraction which is defined as amount of acid site in external section over the amount of total acid site. The external surface fraction is determined by depth that dTBP can penetrated from the surface(0.5nm). Assuming the BASs are evenly distributed. The external acid site fraction

f_{ext} :$external\ acid\ site\ fraction = \frac{volume\ of\ external\ surface\ within\ dTBP\ accessible\ depth*BAS\ density}{total\ volume\ of\ catalyst\ particle*BAS\ density}$

The kinetic rate expression for self-etherification is shown as Equation 2.

$$r_B = \frac{dC_B}{dt} = \frac{k_2 K_B C_A}{(1+K_B C_A)} * C_{H^+} f_{ext} + k_{2int} \overline{C_A} C_{H^+}(1 - f_{ext}) \hspace{1cm} \text{Equation 2}$$

$$\overline{C_A} = \frac{K C_A}{1+K C_A} \overline{C_A^{max}} \hspace{3cm} \text{Equation 3}$$

the kinetic parameter $k_{2\,int}$ represents the effective rate constant of etherification reaction. $\overline{C_A}$ is the concentration of benzyl alcohol adsorbed on the acid site, which is denoted by equation 3. Equation 3 is derived from the Langmuir adsorption isotherm [6]. K is the adsorption equilibrium constant. $\overline{C_A^{max}}$ is the maximum adsorbed concentration of benzyl alcohol. The estimated parameters, which taken from the literature [5]. The diffusivity D_{mA} is taken from diffusion limited data of conventional MFI catalyst. are shown in table 1.

parameters	estimated value
$k1s(/s)$	0.0025 ± 0.0001
$k2(/s)$	0.0013 ± 0.00005
$KB(L/mol)$	3.9 ± 0.1
$k2_{int}(Lcat/[mol/s])$	0.0014 ± 0.0001
$D_{mA}(m^2/s)$	$(4.4 \pm 1.2) * 10^{-20}$
$K(L/mol)$	62
$\overline{C_A^{max}}(mol/L\_cat)$	1.35

Table 1 the parameters of self-etherification and alkylation

The Diffusion models

To simulate the effect of micropore diffusion on the self-etherification reaction, A material balance of benzyl alcohol (A) using Fick's law is applied. Assuming steady state:

$$\nabla \cdot J_A = r_A$$

$$J_A = -D_{mA}\nabla C_A \qquad \text{Equation 4}$$

D_{mA} is the effective diffusion coefficient. J_A is the mass flux of A $\left(\frac{mol}{m^2s}\right)$. r_A is the reaction rate $\left(\frac{mol}{m^3s}\right) = \frac{dC_A}{dt}$.

For the sphere geometry, the material balance can be further derived into equation 5:

$$D_{mA}\left(\frac{d^2C_A}{dR^2} + \frac{2}{R}\right) = -r_A \qquad \text{Equation 5}$$

with boundary condition:

$$\begin{cases} C_A = C_{AS} \ at \ R = radius \ of \ sphere \\ \dfrac{dC_A}{dR} = 0 \ at \ R = 0 \end{cases}$$

C_{AS} is the concentration of benzyl alcohol at the surface, which is equal to 0.17 mol/L

Geometry

In this simulation, the geometry of finned catalyst is assumed as a sphere with cylinder-shape fin which have diameter α and length α. The smallest distance between the edge of two cylinder is defined as fin pitch γ. The diameter of sphere is β. The geometry is shown in figure 3.
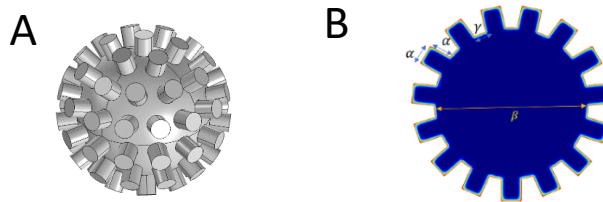

Figure 3 the geometry of catalyst in the simulation(A), with fin dimensions α, interior dimension β, and fin pitch γ (B).

For the geometry design, fin pitch and Interior dimension are two variables considered in this work. catalyst 1 and 2 are geometries that the Rimer's group paper used in Monte carlo simulation. They have same interior dimension β(500nm), and fin dimension α(50nm), while the fin pitches are different (50nm and 25nm, respectively). catalyst 3 4 are possible geometries of catalysts that Rimer's group synthetized.

They have same fin dimension(35nm) and pitch(17.5nm), but the interior dimensions are different (250nm and 390nm, respectively). To evaluate the effect of fin on the mass transfer, conventional spherical catalysts with diameter β+2α and β are simulated and compared with finned catalyst with interior and fin dimension β and α, respectively. The detail of the geometry of finned catalyst is shown in table 2.

Simulation

Equation 4 combining with equation 2 describes the reaction and diffusion model of self-etherification. The model is built on COMSOL software which apply finite element method to solve the problem. Fin part of the catalyst is discretized into "free tetrahedral mesh" with "finer" mesh size. The seed crystal part is discretized with "boundary layer method" due to the uniform shape. The module chosen in the simulation

is 'Transport of diluted species in porous media module'. The specific procedures have been recorded as a video.[23]

geometry	α	γ	β	External acid site fraction for MFI material*	Surface area
catalyst 1*	50nm	50nm	500nm	0.0976	1865800nm^2
catalyst 2*	50nm	25nm	500nm	0.0119	1444600nm^2
catalyst 3	35nm	17.5nm*	250nm	0.0225	470090nm^2
catalyst 4	35nm	17.5nm*	390nm	0.0155	1161500nm^2

Table 2 geometries, external acid site faction & surface areas of finned catalysts

Result and discussion

Validity of the model

The validity of the model is tested via comparing the reaction rates from numerical models with analytical method at different geometries of catalysts. In particular, the reaction rates in the fin region of the numerical model are compared with the analytical reaction rates in cylinder geometry catalysts which have exactly same size to the fin in numerical model. To simplify the calculation process, an isothermal, isobaric first order reaction is assumed:

$$r = k_v C_A \qquad\qquad \text{equation 6}$$

Where $k_v = 0.01 \ s^{-1}$

For diffusion model, fick's law is applied to represents the equimolar flux, which is equation 4. In this case, the Thiele modulus and effectiveness factor for cylinder can be calculated as:[7]

$$\phi = R_p \sqrt{\frac{k_v}{D_{eff}}} \qquad\qquad \text{equation 7}$$

$$\eta = \frac{2I_1(\phi)}{\phi I_0(\phi)} \qquad\qquad \text{equation 8}$$

Where I_i represent modified Bessel function of order i, which is represented by an integral formula [7]:

$$I_i(\phi) = \frac{1}{\pi}\int_0^\pi e^{\phi\cos\theta}\cos i\,\theta d\theta - \frac{\sin i\pi}{\pi}\int_0^\infty e^{-\phi\cosh t - it}dt \qquad\qquad \text{equation 9}$$

According to the definition of effectiveness factor, the analytic solution of reaction rate $r_{analytic}$ can be calculated as:

$$r_{analytic} = \eta * r_{max} = \frac{2I_1(\phi)}{\phi I_0(\phi)} * k_v C_{A0} * V \qquad\qquad \text{equation 10}$$

Where r_{max} is the reaction rate. C_{A0} is the surface concentration. V is the volume of one fin. For the numerical model, we calculate the reaction rate in the volume of one fin of the finned catalyst (shown in Figure 4). For the geometry, the aspect ratio (length/ diameter) is set from 1 to 100. The comparation of the reaction rate is shown in figure 4
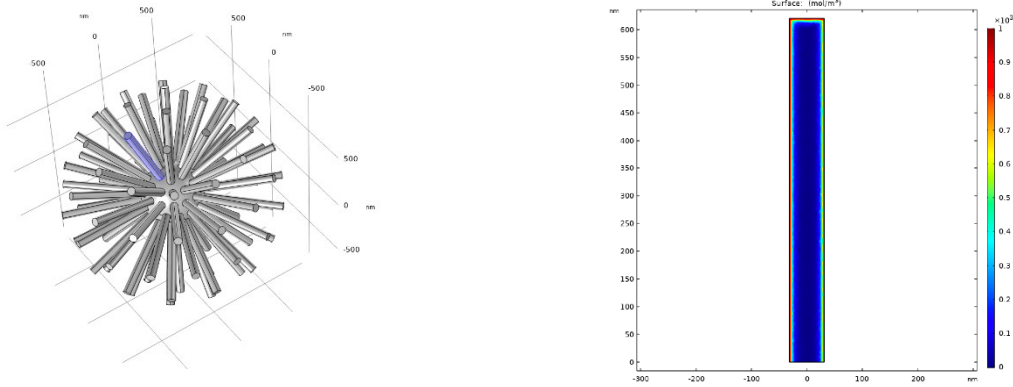
Figure 4 The location of fin (blue region in left figure) where the concentration profile (the right figure) is plotted. The fin has 1:10 aspect ratio
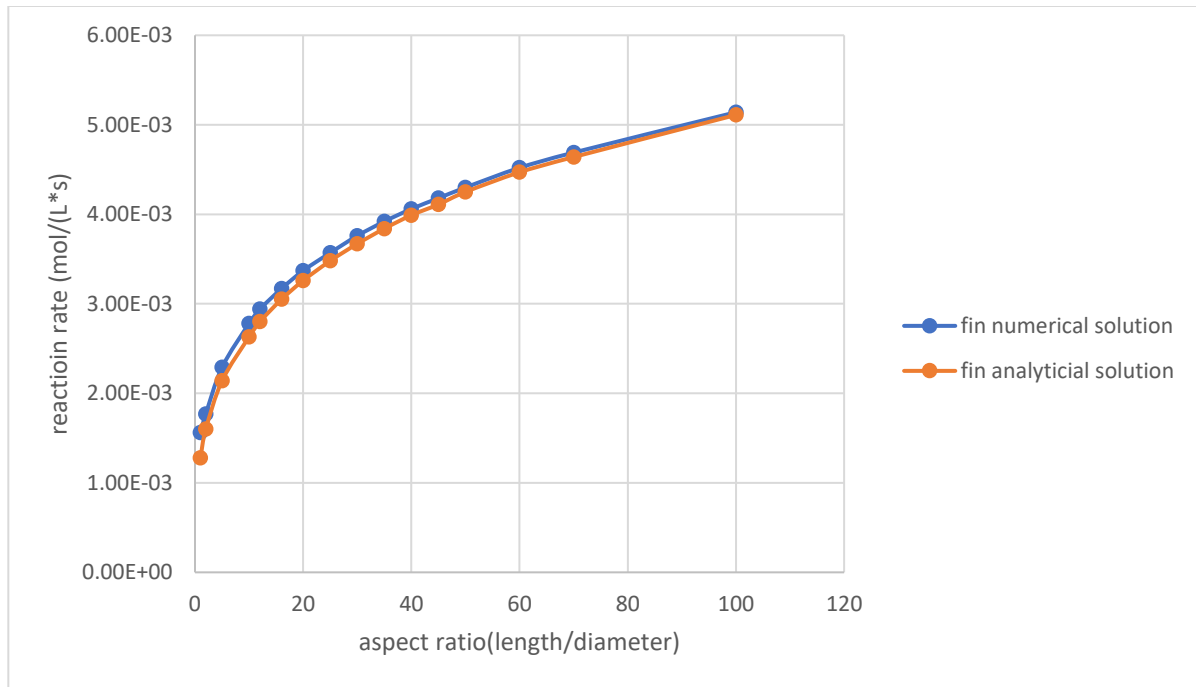
Figure 5 the comparation between analytical solution and numerical solution at aspect ratios from 1 to 100

From the result, it can be seen that the numerical solution and analytical solution agree well to each other. The difference of results can be found at low aspect ratios. This phenomenon can be explained by the difference of boundary condition. In the numerical model, the base area of fin is not contacted to the solution, so the boundary concentration is not applied to this face. Meanwhile, the boundary condition of

8

analytical model includes every faces of the geometry. Therefore, the small aspect ratios result in large base area and therefore large deviation of the result.

Comparation of finned catalysts in different geometries

Comparation between the alkylation and etherification reaction rate for four finned catalyst are shown in Figure 4. The comparation between catalyst 1 and 2 revealed that both the alkylation and etherification reaction rate is increasing with smaller fin pitch (more numbers of fins) on the surface of crystal. From the difference between catalyst 3 and 4. it can be found that the reaction rates are increasing with larger interior dimension. These differences can be explained by larger surface area as the number of fins increases, therefore more accessible acid site in the external surface.
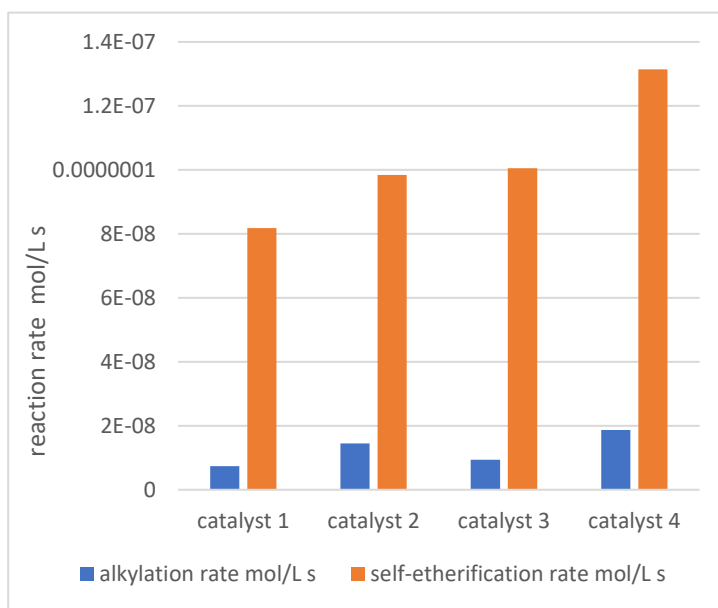

Figure 6 comparations between four finned catalysts

From the comparison between the reaction rates in conventional catalyst and finned catalyst in figure 4, figure 5, and figure 6, it can be seen that the finned catalysts show higher activities than conventional catalyst.
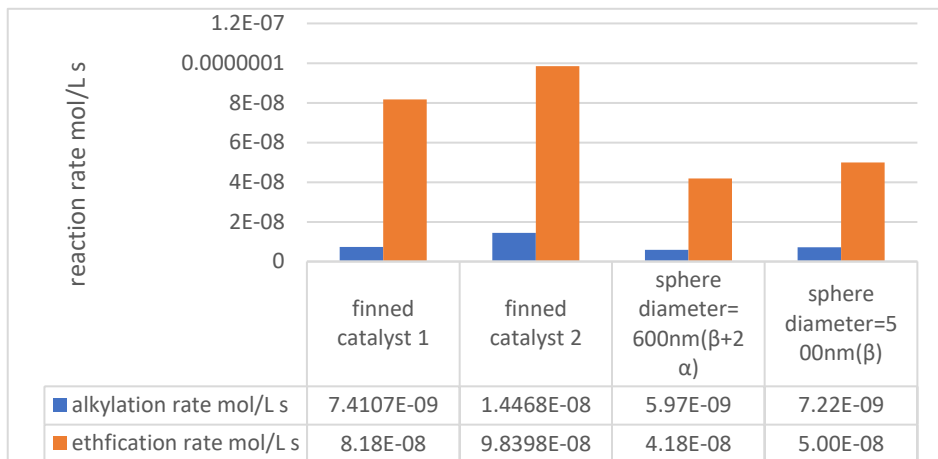
reaction rate mol/L s	finned catalyst 1	finned catalyst 2	sphere diameter= 600nm(β+2α)	sphere diameter=500nm(β)
alkylation rate mol/L s	7.4107E-09	1.4468E-08	5.97E-09	7.22E-09
ethfication rate mol/L s	8.18E-08	9.8398E-08	4.18E-08	5.00E-08

Figure 7 comparations between finned and sphere catalyst with α=50nm β=500nm

reaction rate mol/L s	finned catalyst 3	sphere diameter= 320nm(β+2α)	sphere diameter=250 nm(β)
alkylation rate mol/L s	1.87E-08	1.13E-08	1.44E-08
etherfication rate mol/L s	1.31E-07	7.79E-08	9.92E-08

Figure 8 comparations between finned and sphere catalyst with α=35nm β=250nm

reaction rate mol/L s	finned catalyst 4	sphere diameter=460 nm(β+2α)	sphere diameter= 390nm(β)
alkylation rate mol/L s	1.87E-08	7.85E-09	9.25E-09
etherfication rate mol/L s	1.31E-07	5.44E-08	6.40E-08

Figure 9 comparations between finned and sphere catalyst with α=25nm β=250nm

In figure 7 the selectivity of finned catalysts calculated from the model is plotted against the dimensionless term $\left(\frac{1}{f_{ext}} - 1\right)\eta_m$. The blue line represents e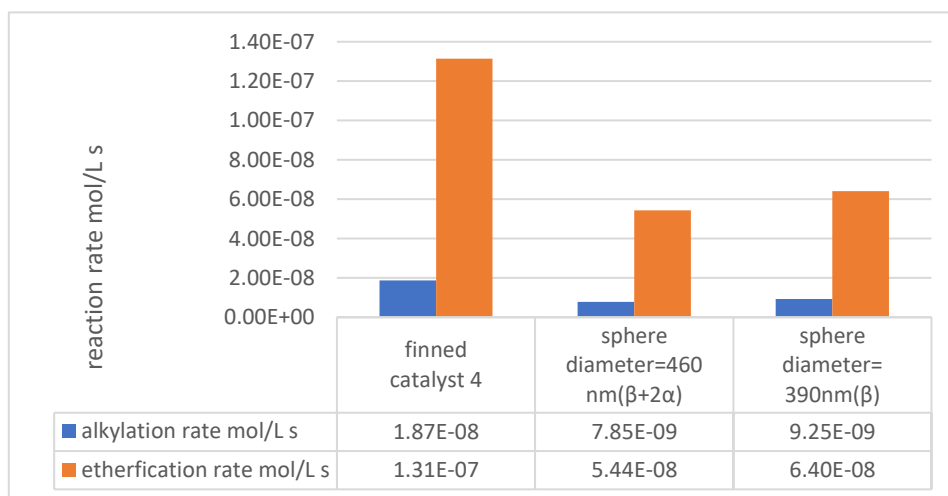xpression of selectivity derived by Dandan et al [5], which is shown by equation 6. The selectivity is defined as the reaction rate of self-etherification over the reaction rate of alkylation. Figure 7 reveals that the simulation result is agreed well with analytical solution.

$$S_{\frac{B}{P}} \sim \left(\frac{k_2 K_B}{k_{1S}}\right) C_{A0} + \left(\frac{k_{2int}}{k_{1s}}\right)\left(\frac{KC_{A0}}{1+KC_{A0}} \overline{C_A^{max}}\right)(1 + K_B C_{A0})\left(\frac{1}{f_{ext}} - 1\right)\eta \qquad \text{Equation 6}$$

$$\eta = \frac{\tanh(\phi)}{\phi}, \phi = x_p\sqrt{2k_{2int}C_{H,int}^+/D_{mA}}$$

$C_{H,int}^+$ denote the BAS concentration inside the catalyst, which is $C_{H,int}^+ = BAS(1 - f_{ext})\rho_{zeolite}$

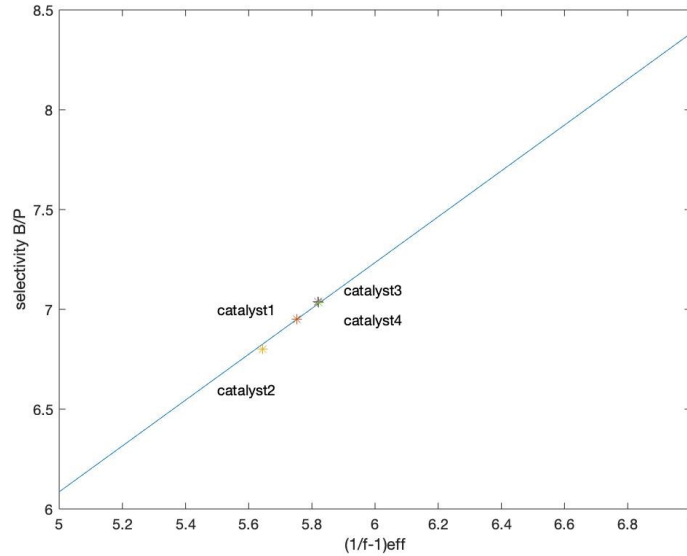η is the effectiveness factor for the first-order self-etherification.

Figure 10 The selectivity as a function of external acid site fraction f$_{ext}$ and the effectiveness factor η$_{m}$.

catalyst 3 and 4 overlap to each other.

The effect of internal mass tranfer limiation can be revealed by the effectiveness vs thiele modulus plot(figure 8). The purple line reperesnts the predicted effectivesss vs thiele modulus calculated by $\eta = \frac{\tanh(\phi)}{\phi}$ The plot shows that there are strong mass transfer limiations inside the four finned catalysts.
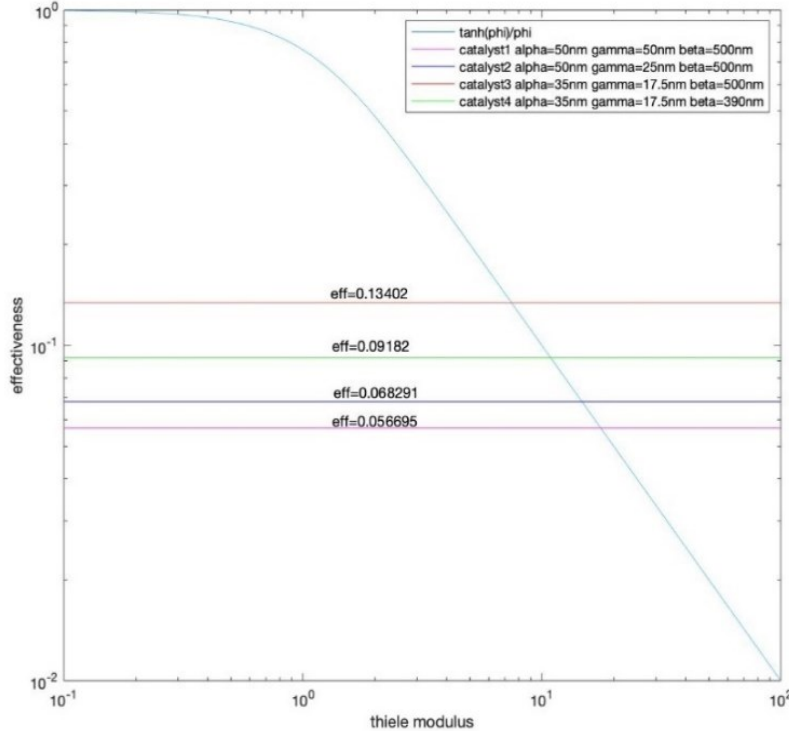
Figure 11 Effectiveness vs Thiele modulus
horizontal lines: Model predication

Conclusion

To reveal the effect of the geometry on the selectivity of the catalyst and diffusion limitation, a reaction-diffusion model with finned sphere geometry catalyst is built via using COMSOL. Two parallel reactions (self-esterification and alkylation) are carried out inside the catalyst to test the selectivity. Simulation results shows that the selectivity will increase with smaller fin pitch (more fin on the surface). The effectiveness factor for the self-esterficaiotion shows that the diffusion limitation is reduced with more Smaller fin pitch (more fins on the surface).

Chapter 2

Introduction

Zeolites are commonly used as catalytic material for many reactions like xylene isomerization, hexane isomerization, amortization, alkylation, and esterification in the industry.[9] During the catalytic process of microporous zeolite crystalline material, the reaction rate are determined by three phenomena happening inside the zeolite particle, diffusion, adsorption, and reaction. The diffusion limitation for different reactant and productions has huge influence on the conversion and reactivity of reaction. The diffusivity is influenced by size of molecules, shape of molecules and configuration [10], For instance, p-xylene can diffuse freely inside the channel of MFI zeolite, however, o-xylene, the isomer of p-xylene, prefer to stay in intersection of channels due to more "leg rooms".[11]. Since there are only 4 intersection per cell in MFI zeolite, the 'infection isotherm' phenomenon [12] will happen if the molar loading larger than 4 molecules per unit cell. In this case, o-xylene molecules will be pushed into somewhere else in the channel, result in additional active site accommodated in the channel with loading increase. This additional push causes the loading dependence of Mexwell-stefan diffusivity. According to Krishna and others' work [13-16], the Diffusivity will decrease with the loading with the relation:

$$D_i = D_i(0)\theta_V \qquad \text{equation 7}$$

$D_i(0)$ is diffusivity with zero loading. θ_V is the fractional occupancy vacancy. This scenario is called the 'strong confinement scenario'.

For large molecules with molar loading smaller than 4 molecule per cell, and other small molecules like He, Ar in MFI, the diffusivity is independent of the loading:

$$D_i = D_i(0)$$

In this thesis, the inter-crystalline diffusion is described by maxwell-Stefan functions. Compare with fick'law, Maxwell-Stefan (MS) model can describe the interaction between each species in a mixture more accurately. For n component mixture, the MS equation is shown as below:[16]

$$\nabla\mu = RT\sum_{j=1}^{n}\frac{\theta_j(u_i-u_j)}{D_{i,j}} + \frac{RTu_i}{D_i}, i = 1,2,\dots n \qquad \text{equation 8}$$

$-\nabla\mu_i$ is chemical potential, which can be interpreted as the force acting on species i which has velocity u_i. The first term on the right-hand side describes the friction force on species i from other species j. $D_{i,j}$ represents the inverse drag coefficient between j and i species. The second term may interpret as the friction between species i and the internal surface of crystal. D_i represents the inverse drag coefficient between adsorbate and surface. θ_j is the fractional occupancy of fractional phase $=\frac{q_i}{q_{sat}}$

The chemical gradient can be related to thermodynamic correction factor in terms of loading by [17]

$$\frac{q}{Rt}\nabla\mu = \sum_{j=1}^{n}\Gamma_{ij}\nabla q_i ; \Gamma_{ij} = \frac{q_i}{p_i}\frac{\partial p_i}{\partial q_j} \qquad \text{equation 9}$$

According to definition of mass flux $N_i = u_i\rho q_i$, velocity u_i can be expressed as $\frac{N_i}{\rho q_i}$. Combining equation 8 and 9, we can get an equation in matrix form

$$\rho\frac{q}{Rt}\nabla\mu = \sum_{j=1}^{n}B_{ij}N_j \qquad \text{equation 10}$$

Where $B_{ii} = \frac{1}{D_i} + \sum_{j=1}^{n}\frac{x_j}{D_{ij}}, B_{ij} = -\frac{x_i}{D_{ij}}, i,j = 1,2\dots.n$
x_i is the mole fractions in the adsorbed phase, which is defined as:
$$x_i = \frac{q_i}{q_1+q_2+\cdots q_n} \qquad \text{equation 11}$$
Equation 10 can be casted into matrix form

$$(N) = -\rho[B]^{-1}[\Gamma]\nabla(q) \qquad \text{equation 12}$$

if there are no interaction between two species (facile exchange), then $D_{ij} \rightarrow \infty$, $[B]^{-1} = \begin{bmatrix} D_1 & 0 \\ 0 & D_2 \end{bmatrix}$

Then for two component system, the flux expression can be simplified to

$$N_1 = -\rho D_1[\Gamma_{11}\nabla q_1 + \Gamma_{12}\nabla q_2] = -\rho D_1 \left[\frac{q_1}{p_1}\frac{\partial p_1}{\partial q_1}\nabla q_1 + \frac{q_1}{p_1}\frac{\partial p_1}{\partial q_1}\nabla q_2\right] \qquad \text{equation 13}$$

$$c = -\rho D_2[\Gamma_{21}\nabla q_1 + \Gamma_{22}\nabla q_2] = -\rho D_2 \left[\frac{q_2}{p_2}\frac{\partial p_2}{\partial q_1}\nabla q_1 + \frac{q_2}{p_2}\frac{\partial p_2}{\partial q_2}\nabla q_2\right] \qquad \text{equation 14}$$

if mass flux equations are expressed in term of pressure p_i

$$N_1 = -\rho D_1 \left[\frac{q_1}{p_1}\nabla p_1\right] \qquad \text{equation 15}$$

$$N_2 = -\rho D_2 \left[\frac{q_2}{p_2}\nabla p_2\right] \qquad \text{equation 16}$$

The relationship between partial pressure p and loading q is described by adsorption model. In this thesis, multicomponent Langmuir isotherm and Ideal adsorption theory (IAST) with single component Langmuir isotherm are considered as adsorption models. Multicomponent Langmuir adsorption model (MCL)is shown below:

$$q_i = \frac{q_{isat}b_ip_i}{1+\sum_{i=1}^{i=n}b_ip_i} \qquad \text{equation 17}$$

b_i is the Langmuir adsorption constant. $q_{i_{Sat}}$ is the saturated loading of each species.

IAS theory is proposed by Myers and Prausnitz in 1965[18]. It is a thermodynamic consist model for predict the adsorption equilibria of mixture. The equation of IAS theory is analogue to Raoult's law:

$$p_i = P_i^0 x_i \qquad \text{equation 18}$$

p_i is the partial fugacities in the bulk fluid phase. P_i^0 is the pressure for sorption of every component i, which yields the same spreading pressure, π for each of the pure component. Therefore, for each component:

$$\frac{\pi A}{RT} = \int_0^{P_1^0} \frac{q_1^0(f)}{f} df = \int_0^{P_2^0} \frac{q_2^0(f)}{f} df = \cdots \int_0^{P_n^0} \frac{q_n^0(f)}{f} df \qquad \text{equation 19}$$

where q_i^0 is the pure component adsorption isotherm, which can be described by single or multi-site Langmuir isotherm.

A key assumption of the IAST is that the enthalpies and surface areas of the adsorbed molecules do not change upon mixing:

$$\frac{A}{q_t} = \frac{Ax_1}{q_1^0(P_1^0)} + \frac{Ax_2}{q_2^0(P_2^0)} + \cdots \frac{Ax_n}{q_n^0(P_n^0)} \qquad \text{equation 20}$$

Where the total loading $q_t = q_1 + q_2 + \cdots q_n$. $q_i^0(P_i^0)$ are determined from pure component adsorption isotherm. $\frac{A}{q_t}$ represents the surface area covered by adsorbents. The equation15-17 need to be solved together to find the relation between p_i and q_i. Especially, when the saturation loading q_{sat} of every species are the same, IAST model will be same as Multicomponent Langmuir model. Langmuir-Hinshelwood (LH) mechanism are commonly used to explain the surface reaction in the catalyst. Generally, this mechanism considers the reaction rate depend on the number of densities of adsorbed molecules on the catalyst surfaces.[19] For a reversible isomerization reaction $A(1) \leftrightarrow B(2)$ The global reaction rate equation is shown below:

$$r = k_1^\theta \theta_1 - k_2^\theta \theta_2 = k_1 q_1 - k_2 q_2 = (k_1^p p_1 - k_2^p p_2)\theta_v \qquad \text{equation 21}$$

Where θ_1 and θ_2 is the fractional loading occupancy, which is defined as $\frac{q_1}{q_{sat}}$ and $\frac{q_2}{q_{sat}}$. The relationship between k_i^p and k is explained by MCL isotherm or IAST model.

In this thesis, we choose a MCL-LH model example and an IAST-LH model example from two Krishna's papers [20][21] to prove the validity of our model. All parameters are from the same paper.

Modelling

Effectiveness factor of catalyst with MCL-LH model

An isomerization reaction 2-methylpentane $2MP(1) \leftrightarrow 2,2$ dimethyl-butane $22DMB(2)$ in MFI zeolite is considered for modelling.[20] The kinetic rate equation can be written as

$$R_{kg} = k_1 q_1 - k_2 q_2 \qquad \text{equation 22}$$

where k_1 and k_2 is reaction rate constant 1/s. The unit of R_{kg} is $mol\ kg\ catalyst^{-1} s^{-1}$

Under steady state, the continuity equation for diffusion and reaction in the spherical zeolite crystalline with radius r_1 is shown below:

$$\frac{1}{r^2}\frac{\partial}{\partial r}(r^2 N_i) = \rho v_i R_{kg} \qquad \text{equation 23}$$

Where $v_1 = -1, v_2 = 1. R_{kg} = k_1 q_1 - k_2 q_2$

If multicomponent Langmuir model (equation 14) is applied, the mass flux equation 12 and 13 can be further simplified into

$$N_i = -\rho D_i \sum_{j=1}^{n} \Gamma_{ij} \frac{\partial q_j}{\partial r} \qquad \text{equation 24}$$

Where thermodynamic correction factor equal

$$\Gamma_{ij} = \delta_{ij} + \frac{q_i}{q_{j,sat}\theta_v} \qquad \text{equation 25}$$

δ_{ij} is the Kronecker delta. θ_v is the occupancy vacancy fraction $=1 - \frac{q1}{q_{sat}} - \frac{q2}{q_{sat}}$

The effectiveness factor η is

$$\eta = \frac{\int_0^r R_{kg} r^2 dr}{R_{kg}\int_0^r r^2 dr} \qquad \text{equation 26}$$

If Fick's law is applied, the thermodynamic correction factor is further simplified to $\Gamma_{ij} = \delta_{ij}$

And the mass flux become $N_i = -\rho D_i \frac{\partial q_i}{\partial r}$ $\qquad \text{equation 27}$

Strong

The analytical solution of the effectiveness factor can be found from textbook [19]

$$\eta = \frac{1}{\phi}\left(\frac{1}{\tanh(3\phi)} - \frac{1}{3\phi}\right) \qquad \text{equation 28}$$

17

The corresponding Thiele modulus

$$\phi = \frac{r_c}{3}\sqrt{\frac{k_1}{D_1(0)} + \frac{k_2}{D_2(0)}}$$

equation 29

The partial pressures at the surface of the catalyst are 10kPa for both 22DMB and 2MP. The corresponding loading at the surface of catalyst can be calculated via MCL model. Then the boundary condition for two differential equations become

$$\begin{cases} q_1 = 0.1655 \frac{mol}{kg}, at\ r = r_1 \\ \frac{\partial q_1}{\partial r} = 0, at\ r = 0 \end{cases} \begin{cases} q_2 = 0.29 \frac{mol}{kg}, at\ r = r_1 \\ \frac{\partial q_2}{\partial r} = 0, at\ r = 0 \end{cases}$$

The value of parameter $k_1, k_2, D_1, D_2\ b_1, b_2$ comes from Krishna's work [20].

parameters	estimated value
Reaction rate constant k_1	$0.0011 s^{-1}$
Reaction rate constant k_2	$0.00055 s^{-1}$
$\dfrac{D_1}{r_1}$	$0.005 s^{-1}$
$\dfrac{D_2}{r_2}$	$0.0000625 s^{-1}$
b_1	$0.000127\ Pa^{-1}$
b_2	$0.0000712\ Pa^{-1}$

Table 3 parameters for MCL-LH model

Effectiveness factor of catalyst with IAST-LH model

For the IAST-LH model, we choose an example from Krishna's paper [21]. A reversible isomerization $nC6$(n-hexane)$(1) \leftrightarrow 22$DMB(2,2-dimethylbutane) (2) reacts inside the spherical MFI catalyst. The continuity equation is same as equation 22, where N_1 and N_2 is expressed as equation 14 and 15.

The reaction equation is $R_{kg} = k_1 q_1 - k_2 q_2$. The IAST model applies the equation 15-17. Equation 15 become

$$p_1 = P_1^0 x_1$$

equation 30

18

$$p_2 = P_2^0 x_2$$

<div align="right">equation 31</div>

Equation 16 become

$$\int_0^{P_1^0} \frac{q_1^0(f)}{f} df = \int_0^{P_2^0} \frac{q_2^0(f)}{f} df$$

<div align="right">equation 32</div>

Equation 17 become

$$q1 + q2 = \frac{1}{\frac{x_1}{q_1^0(P_1^0)} + \frac{x_2}{q_2^0(P_2^0)}}$$

<div align="right">equation 33</div>

A double site Langmuir isotherm (equation 30) is used to describe the pure adsorption

isotherm $q_i^0(P_i^0)$ with parameters shown in table 4.

$$q_i^0(P_i^0) = \frac{q_{i,sat,A} b_{i,A} P_i^0}{1 + b_{i,A} P_i^0} + \frac{q_{i,sat,B} b_{i,B} P_i^0}{1 + b_{i,B} P_i^0}$$

<div align="right">equation 34</div>

Component	Temperature(K)	Site A		Site B	
		$b_{i_A}(Pa^{-1})$	$q_{i,sat,A}$ (moecules per unit cell)	$b_{i,B}(Pa^{-1})$	$q_{i,sat,B}$
nC6	362K	0.0632	4	0.0017	4
2DMB	362K	0.01085	4	-	-

Table 4 Dual-site Langmuir parameters for nC6 and 2DMB

To transfer the unit of $q_{i_{sat,A}}$ to $\frac{mol}{kg}$, the number in table 4 need to be multiplied by 0.17337.

[20] All parameters in this model comes from the Krishna's paper [21]. Generally, zero loading

diffusivity $\frac{D_1(0)}{D_2(0)}$=10.Kinetic constant $\frac{k_1}{k_2} = 2$ the bulk partial pressure at the surface of catalyst

$p_1 = p_2 = 10kPa$.

The effectiveness factor for the numerical solution is calculated via equation 22. The Thiele

modulus is defined as

$$\phi = \frac{r}{3}\sqrt{\frac{k_1}{b_1 D_1} + \frac{k_2}{b_2 D_2}}$$

<div align="right">equation 35</div>

Simulation method

COMSOL software with "general form PDE interface" is used for solving the differential equations numerically. A 3-D sphere geometry is built. Normal sized mesh is applied to discretize the model. For IAST-LH model, firstly the IAST theory (equation 26 to 30) is solved via MATLAB to find the expression loading q_i in terms of partial pressure f_i. Then the expressions are inputted into the COMSOL.

Simulation result

The concentration profile and effectiveness factor via simulating MCL-LH model is shown below. We try three different scenarios: strong confinement scenario with MS model, weak confinement scenario with MS model and fick's law model. The loading profile and effectiveness factor calculated in Krishna's paper can be found in supplementary information. The difference between three scenarios shows the thermodynamic coupling effect on the diffusion. The agreement between our results and Krishna's paper proves the validity of our model.
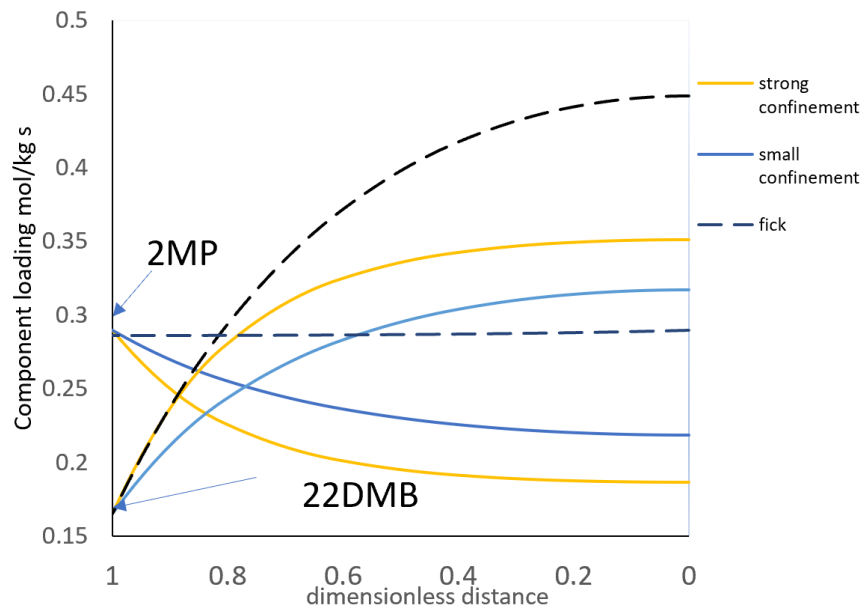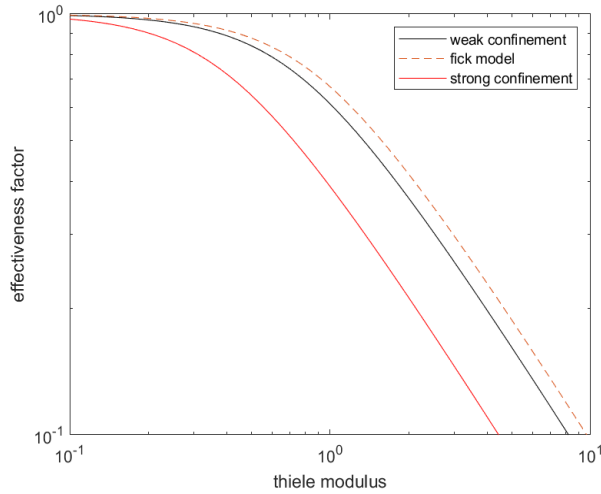

**Figure 12 loading profile along the radial direction when Thiele modulus=1.0011**

Figure 13 effectiveness factor when partial pressure at the surface of crystal p1=p1=10kPa k1/k2=2 D1/D2=80

For the IAST-LH model, firstly we compare the predication of component fugacity as a function of fractional occupancy vacancy 1- θ_{nc6}- θ_{22DMB} via using IAST approach and MCL approach. The ratio of the loading of nC6 and 2DMB is kept at 3. From figure 14, When the vacancy 0.1,0.2.0.9, the effectiveness factor of IAST-LH model and MCL-LH model is shown in figure 15. The significance difference of two model can be found when the vacancy is small (loading is high). This phenomenon is due to the configurational entropy effect [21][22]. The results from our model are same as results calculated in Krishna's paper (see supplementary information.)
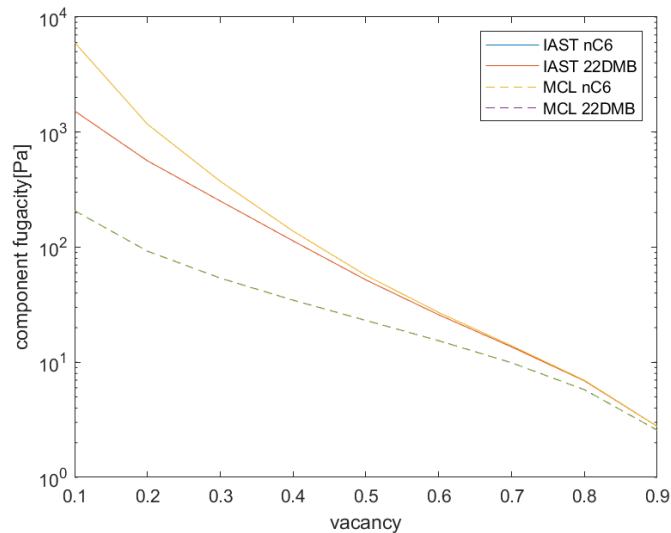
Figure 14 Compare MCL and IAST model: component fugacity vs fractional vacancy $(1 - \theta_{nc6} - 3\theta_{22DMB})$ when loading $\theta_{nc6} = 3\theta_{2DMB}$
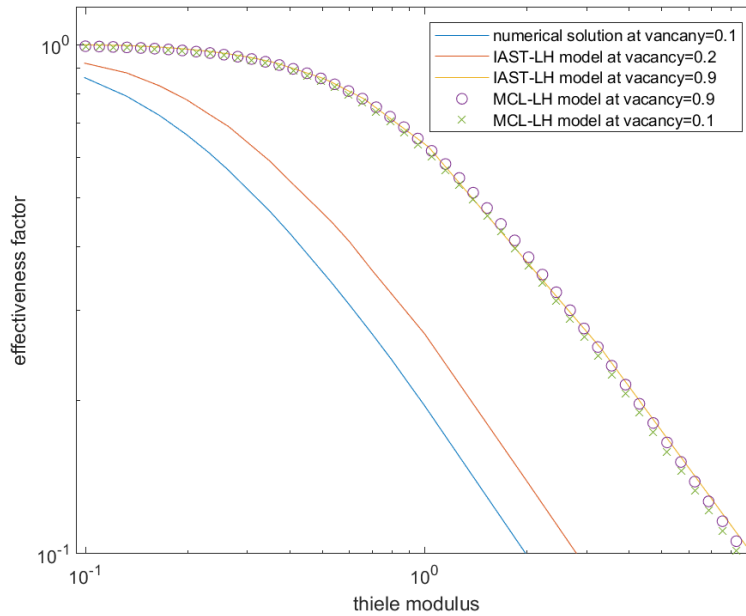
Figure 15 effectiveness factor for weak confinement scenario vis simulating IAST-LH model and MCL-LH model. The fractional loading at the surface is kept at $\theta_{s,nC6} = 3\theta_{s,22DMB}$.

Conclusion

Two reaction- diffusion models with different adsorption mechanisms (MCL and IAST) are formulated via using COMSOL software. For MCL-LH model, three different scenarios (weak confinement scenario, strong confinement scenario and ficken scenario) are simulated. The difference between IAST-LH approach and MCL-LH approach at low vacancy (high loading) is shown via plotting component fugacity and effectiveness at different fractional fugacity. Due to the advantage and simplicity of COMSOL software, this model may be applied to catalyst crystal with odd geometry and couple with complex scenario in reactor simulation.

Supplementary material

1.simulation results of 4 finned catalysts

α=50nm β=500nm	finned catalyst 1	finned catalyst 2	sphere diameter= 600nm(β+2α)	sphere diameter=500nm(β)
effectiveness factor	0.056695	0.068291	0.028857	0.034524
selectivity	6.9499	6.8011	7.0058	6.9256
alkylation rate mol/L s	7.4107E-09	1.4468E-08	5.97E-09	7.22E-09
etherification rate mol/L s	8.18E-08	9.8398E-08	4.18E-08	5.00E-08
External fraction	0.009761005	0.011952945	4.95E-03	0.005988008

Table S1 simulation results for the effectiveness factor, alkylation rate, etherification rate and external fraction for four finned catalysts.

2.Comparation between finned and sphere catalysts

α=50nm β=500nm	finned catalyst 1	finned catalyst 2	sphere diameter= 600nm(β+2α)	sphere diameter=500nm(β)
effectiveness factor	0.056695	0.068291	0.028857	0.034524
selectivity	6.9499	6.8011	7.0058	6.9256
alkylation rate mol/L s	7.4107E-09	1.4468E-08	5.97E-09	7.22E-09
etherification rate mol/L s	8.18E-08	9.8398E-08	4.18E-08	5.00E-08
fraction	0.009761005	0.011952945	4.95E-03	0.005988008

Table S2 comparations between finned and sphere catalysts with α=50nm β=500nm

α=35nm β=390nm	finned catalyst 4	Sphere diameter=460nm(β+2α)	sphere diameter= 390nm(β)
effectiveness factor	0.09182	0.037568	0.044286
selectivity	7.0416	6.9306	6.9218
alkylation rate mol/L s	1.87E-08	7.85E-09	9.25E-09
etherification rate mol/L s	1.31E-07	5.44E-08	6.40E-08
fraction	0.015531564	0.006507572	0.007672601

Table S3 comparations between finned and sphere catalyst with α=35nm β=390nm

α=35nm β=250nm	finned catalyst 3	sphere diameter= 320nm(β+2α)	sphere diameter=250nm(β)
effectiveness factor	0.09182	0.053937	0.068855
selectivity	7.0416	6.9099	6.8808
alkylation rate mol/L s	1.87E-08	1.13E-08	1.44E-08
etherification rate mol/L s	1.31E-07	7.79E-08	9.92E-08
fraction	0.015531564	0.009345734	0.011952064

Table S4 comparations between finned and sphere catalyst with α=35nm β=250nm
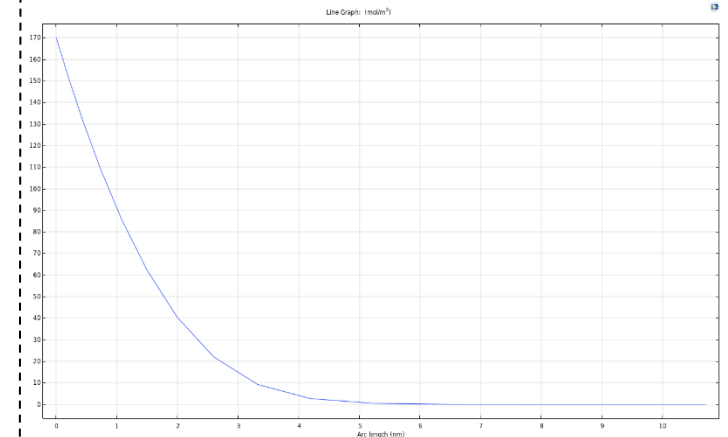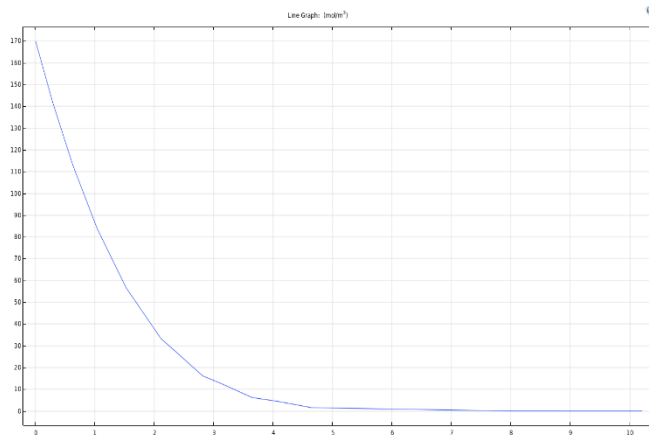
2-D Concentration profile for benzyl alcohol

Catalyst 1 $\alpha = 50nm \, \gamma = 50nm \, \beta = 500nm$ Catalyst 2 $\alpha = 50nm \, \gamma = 25nm \, \beta = 500nm$
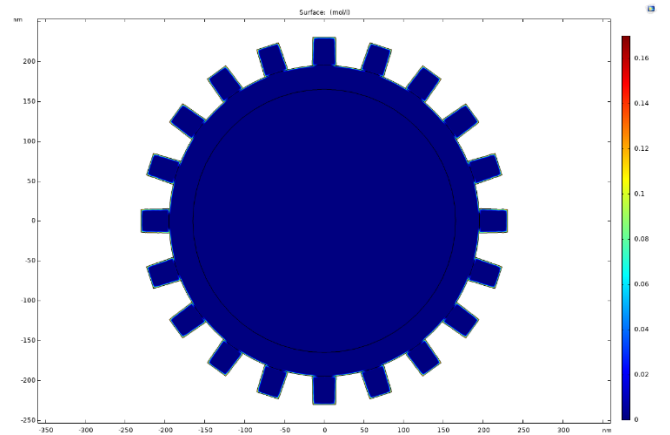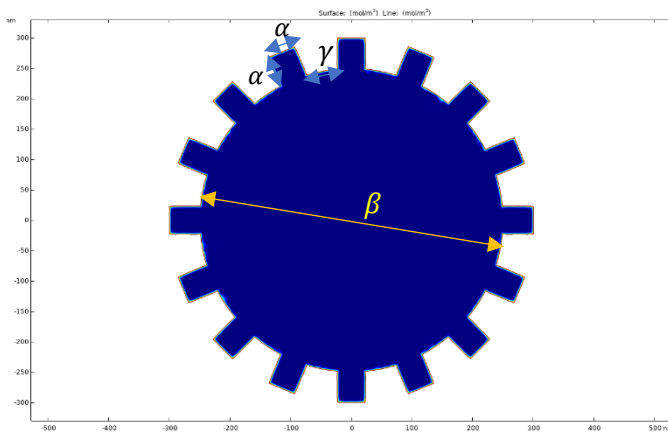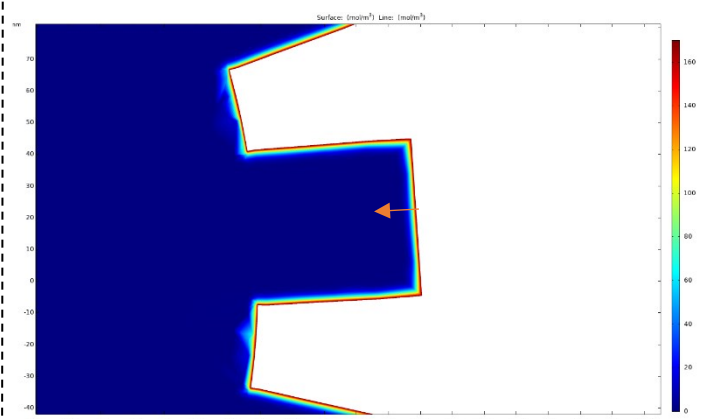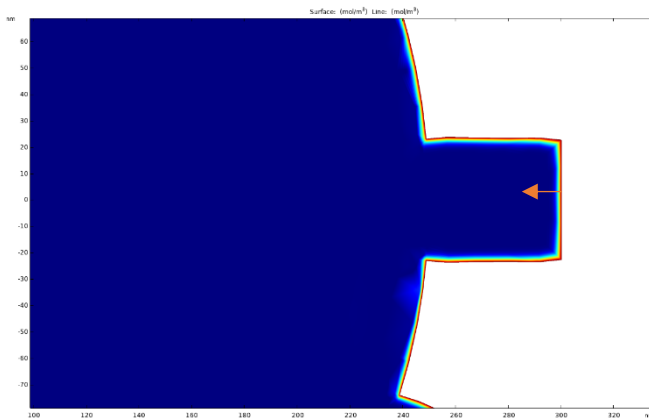

1D Concentration profile from the surface of fin to about 10nm depth in radial direaction

Catalyst 1 $\alpha = 50nm \, \gamma = 50nm \, \beta = 500nm$ Catalyst 2 $\alpha = 50nm \, \gamma = 25nm \, \beta = 500nm$

The location where the profile is plotted:

Comparation of concentration profiles between catalyst 1 and catalyst 2

2-D Concentration profile

Catalyst 3 $\alpha = 35nm$ $\gamma = 17.5nm$ $\beta = 250nm$ Catalyst 4 $\alpha = 35nm$ $\gamma = 17.5nm$ $\beta = 390nm$

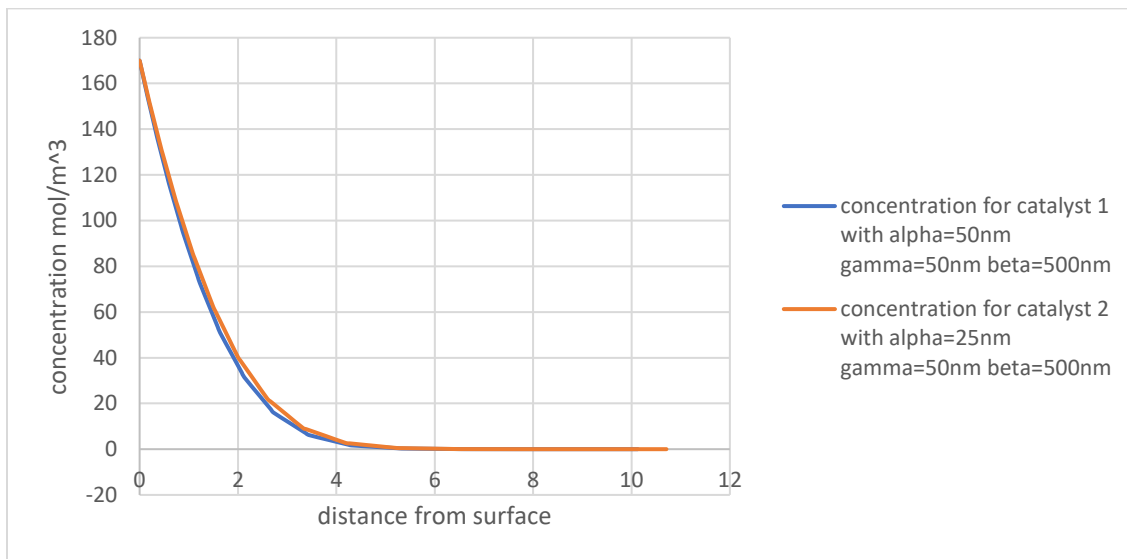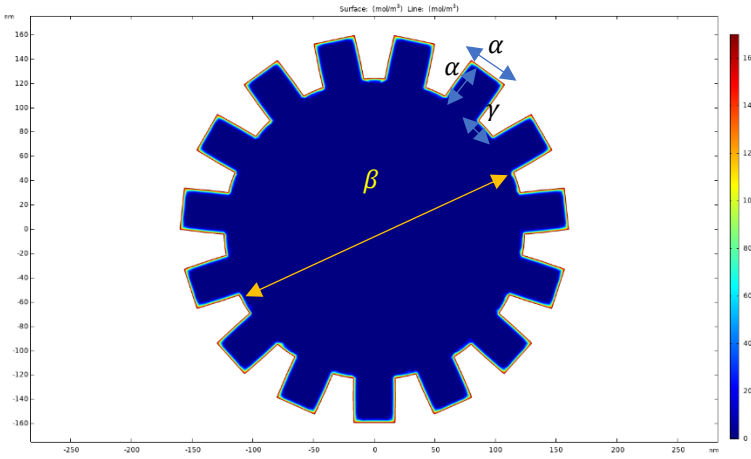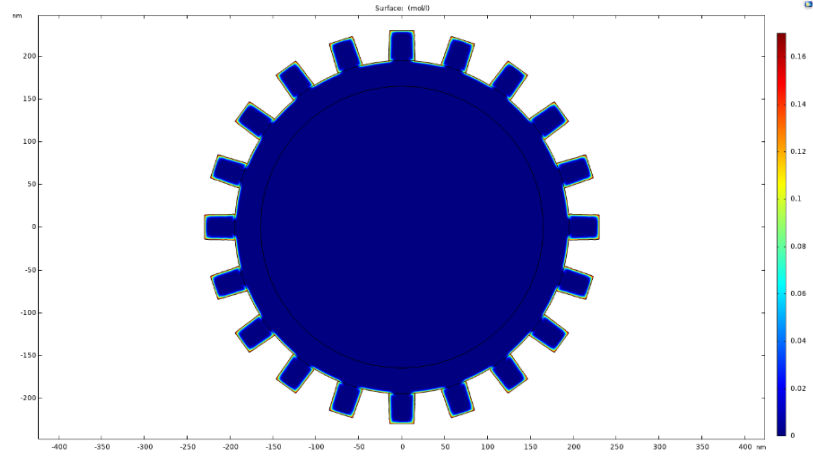## 1D Concentration profile from the surface of fin to about 10nm depth in radial direaction

Catalyst 3 $\alpha = 35nm$ $\gamma = 17.5nm$ $\beta = 250nm$ Catalyst 4 $\alpha = 35nm$ $\gamma = 17.5nm$ $\beta = 390nm$

The location where the concentration profile is plotted   The location where the concentration profile is plotted:
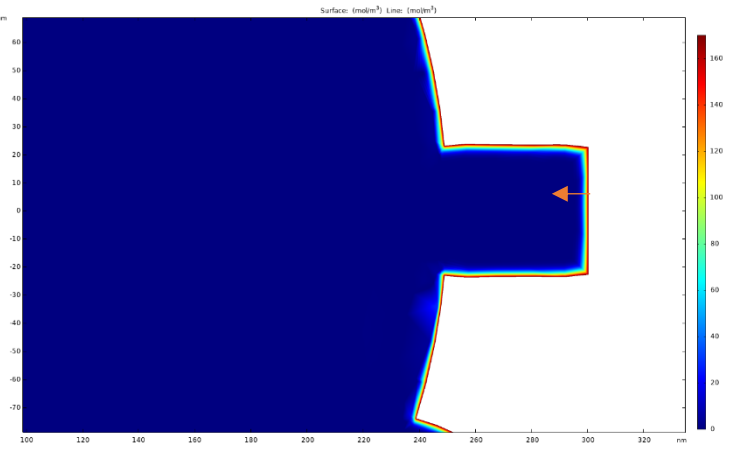
Comparation of concentration profiles between catalyst 3 and catalyst 4

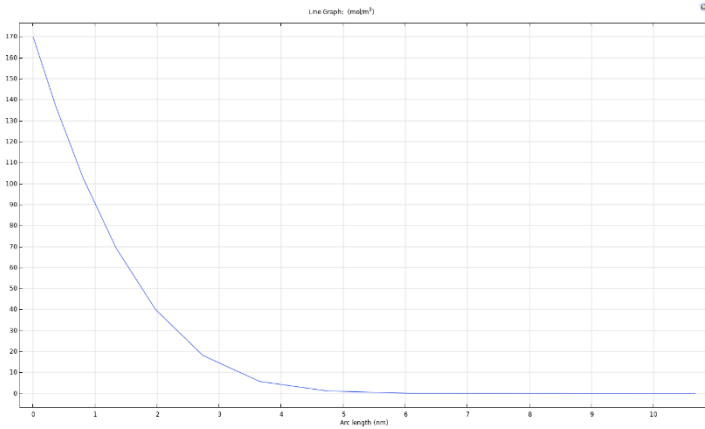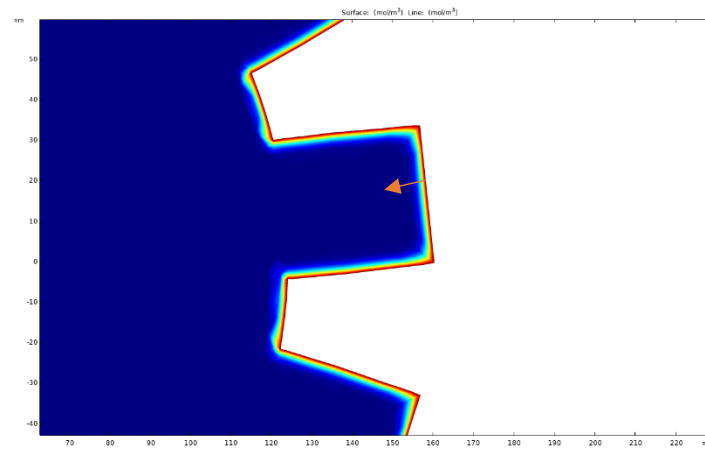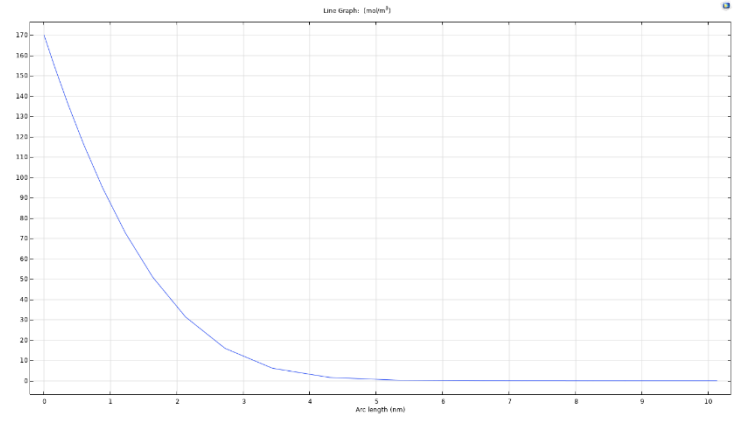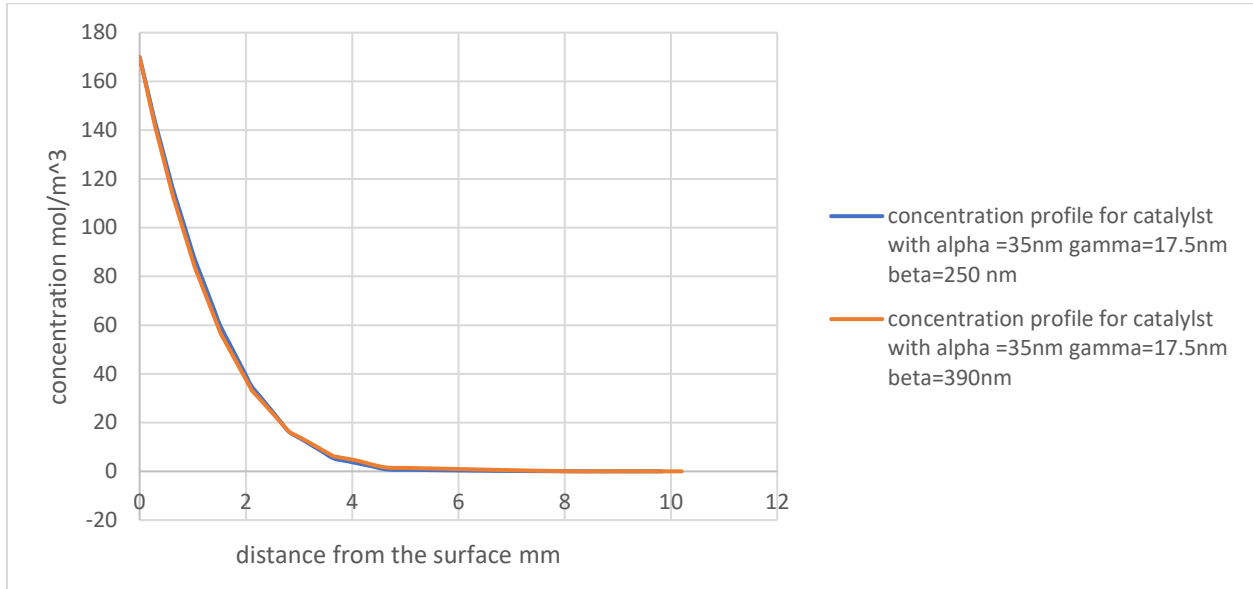| aspect ratio(length/diameter)	length of fin (nm)	radius of fin (nm)	fin analyticial solution(mol/(L s))	fin numerical solution(mol/(L s))
1	135	67.8	0.00128	0.00156
2	214.31	53.6	0.0016	0.00177
5	394.76	39.48	0.00214	0.00229
10	620	31.5	0.00263	0.00278
12	707.64	29.48	0.0028	0.00294
16	857.24	26.79	0.00305	0.00317
20	994.7	24.87	0.00326	0.00337
25	1154.3	23.1	0.00348	0.00357
30	1303.5	21.7	0.00367	0.00376
35	1444.6	20.6	0.00384	0.00392
40	1579	19.7	0.00399	0.00406
45	1708	19	0.00411	0.00418
50	1832.3	18.3	0.00425	0.0043
60	2069	17.2	0.00447	0.00452
70	2293	16.4	0.00464	0.00469
100	2908.6	14.5	0.00511	0.00514

Table S5 comparation between analytical solution and numerical solution at different aspact ratios

The reference results of MCL-LH model in Krishna's paper[20]

a) Calculation of the effectiveness factor, η, for MFI catalyst carrying out the 2MP(1) ⇌ 22DMB(2) reaction at 473 K.

c) The loading profile along the radial direction

(a)

$2MP(1) \rightleftarrows 22DMB(2)$

MFI catalyst; 473 K;
$k_1/k_2 = 2$;
$Đ_1(0)/Đ_2(0)=80$;
$p_1 = p_2 = 10$ kPa;

Effectiveness factor, η

Fick model,
with $\Gamma_{ij}=\delta_{ij}$
M-S model:
weak confinement
M-S model:
Strong confinement

Classic Thiele modulus, φ

(B)

Fick model: $\Gamma_{ij}=\delta_{ij}$
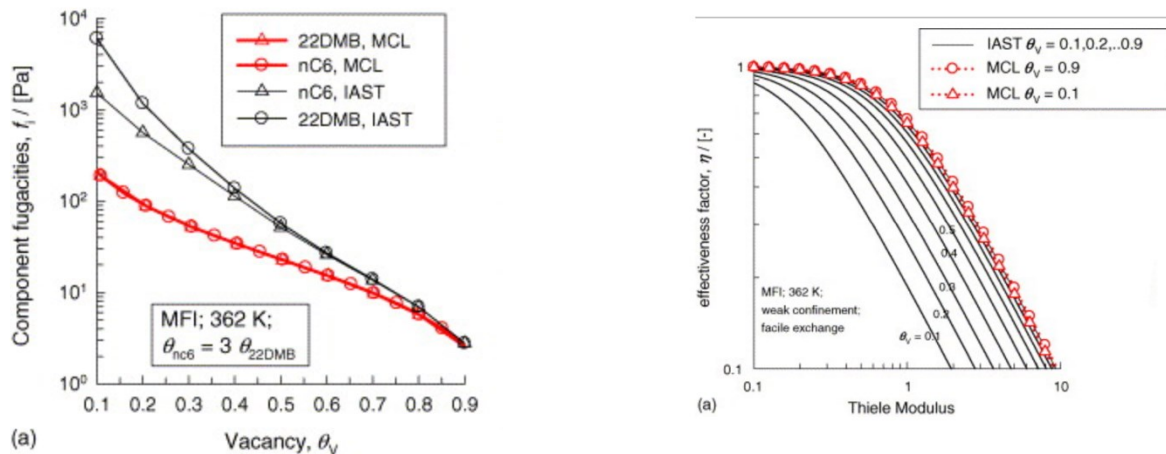M-S model, weak confinement
M-S model, strong confinement

Component loading / mol kg^{-1}

2MP

MFI catalyst; 473 K;
$k_1 = 0.0011$ s^{-1}; $k_1/k_2 = 2$;
$\phi = 1.0011$; $p_1=p_2=10$ kPa

22DMB

dimensionless distance, $\xi = r / r_c$
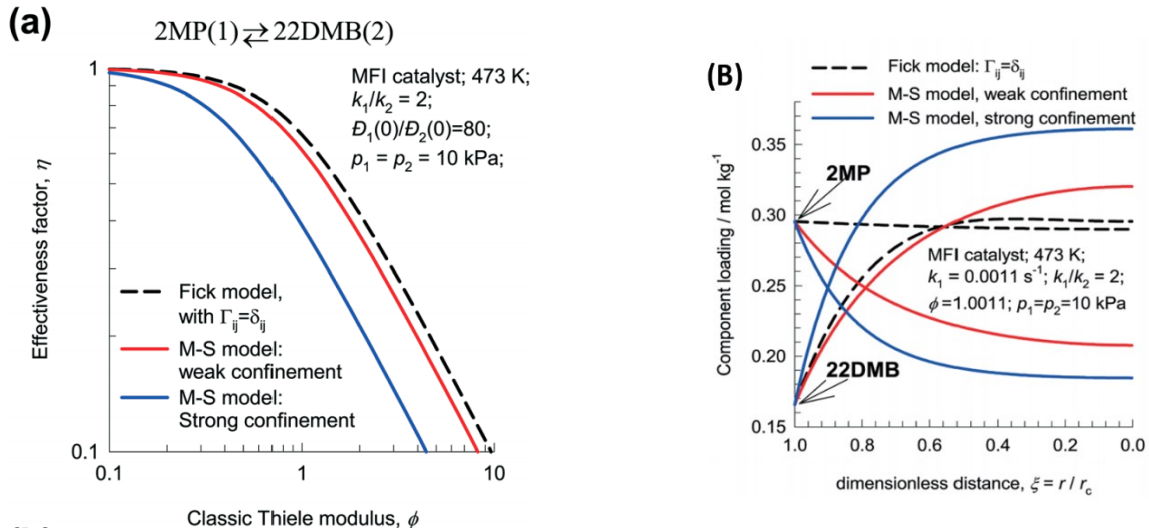
The reference results of IAST-LH model in Krishna's paper [21]

a) Fugacity (partial pressure) f_i of nC6 and 22DMB as a function of the vacancy $\theta_V = 1 - \theta_{nC6} - \theta_{22DMB}$.

b) Effectiveness versus Thiele modulus at weak confinement scenario and facile exchange $Đ_{ij} \to \infty$. The fractional loadings at the surface of the zeolite crystal is fixed with $\theta_{s,nC6} = 3\theta_{s,22DMB}$. Fractional occupancy varies from 0.1 to 0.9.

Component fugacities, f_i / [Pa]

22DMB, MCL
nC6, MCL
nC6, IAST
22DMB, IAST

MFI; 362 K;
$\theta_{nc6} = 3\ \theta_{22DMB}$

(a)

Vacancy, θ_V

IAST θ_V = 0.1,0.2,..0.9
MCL θ_V = 0.9
MCL θ_V = 0.1

effectiveness factor, η / [-]

MFI; 362 K;
weak confinement;
facile exchange
$\theta_V = 0.1$

(a)

Thiele Modulus

28

MATLAB code for solving IAST theory to find the expression of qi in terms of fi

```
syms x1 x2 qt q1 q2 f1 f2
%x1 is the mole fraction of 2-methylpentane in the adsorbed phase
%x2 is the mole fraction of dimethyl-butane in the adsorbed phase
%f1 is the partial pressure of 2-methylpentane
%f2 is the partial pressure of dimethyl-butane
%qt is the total loading ins the adsorbed phase
%q1 is the loading of 2-methylpentane in the adsorbed phase
%q2 is the loading of dimethyl-butane in the adsorbed phase
q1sa=0.6935% mol/kg the saturated adsorption loading of 2-
methylpentane at site A  4*0.17337
q1sb=0.6935% mol/kg the saturated adsorption loading of 2-
methylpentane at site B  4*0.17337
q2sa=0.6935% mol/kg the saturated adsorption loading of dimethyl-
butane at site A  4*0.17337
b1a=0.0632 %pa^-1
b1b=0.0017 %pa^-1
b2a=0.01085%pa^-1
f=(x1)/((q1sa*b1a*f1/(x1))/(1+b1a*f1/(x1))+q1sb*b2a*f1/(x1)/(1+b1b*f1/
(x1)))+(x2)/(q2sa*b2a*f2/(x2)/(1+b2a*f2/x2))-1/(qt); %combination of
equation 32 & 33
g=q1sa*log(1+b1a*f1/x1)+q1sb*log(1+b1b*f1/x1)-
0.6935*log(1+b2a*f2/x2); %equation 31
h=x1+x2-1
n=q1-x1*qt%equation 11
j=q2-x2*qt% equation 12
[x10,x20,qt0,q1,q2]=solve(f,g,h,n,j,x1,x2,qt,q1,q2)
[q1]=simplify(q1)
[q2]=simplify(q2)
```

Literature cited

[1] A. Hwang et al., (2019). Effects of diffusional constraints on lifetime and selectivity in methanol   to-olefins catalysis on HSAPO-34. J. Catal. 369, 122-132

[2] H. Awala et al., (2015).Template-free nanosized faujasite-type zeolites. Nat. Mater. 14, 447-451

[3] K. A. Cychosz, R. Guillet-Nicolas, J. Garcia-Martinez, M. Thommes, (2017).Recent advances in the textural characterization of hierarchically structured nanoporous materials. Chem. Soc. Rev. 46, 389-414

[4] Dai, H., Shen, Y., Yang, T. et al. (2020). Finned zeolite catalysts. Nat. Mater. **19,** 1074–1080

[5]Xu, D., Abdelrahman, O., Ahn, S. H., Guefrachi, Y., Kuznetsov, A., Ren, L., . . . Tsapatsis, M. (2019). A quantitative study of the structure–activity relationship in hierarchical zeolites using liquid-phase reactions. AIChE Journal, 65(3), 1067-1075. doi:10.1002/aic.16503

[6] Zhang X, Liu D, Xu D, et al. (2012) Synthesis of self-pillared zeolite Nanosheets by repetitive branching. Science.;336:1684-1687.

[7] Davis, Mark E. and Davis, Robert J. (2003) Fundamentals of chemical reaction engineering. McGraw-Hill chemical engineering series. McGraw-Hill Higher Education , New York, NY. ISBN 007245007X.

[8] MILNE-THOMSON, L. (1945). A Treatise on the Theory of Bessel Functions. Nature **156,** 190–191 https://doi.org/10.1038/156190a0

[9] Degnan, T. F. (2003). The implications of the fundamentals of shape selectivity for the development of catalysts for the petroleum and petrochemical industries. Journal of Catalysis, 216(1-2), 32-46. doi:10.1016/s0021-9517(02)00105-7

[10] Davis, M. E. (1991). Zeolites and Molecular SIEVES: Not just ordinary catalysts. Industrial & Engineering Chemistry Research, 30(8), 1675-1683. doi:10.1021/ie00056a001

[11] Gupta, A.; Clark, L. A.; Snurr, R. Q. (2000). Grand canonical Monte Carlo simulations of nonrigid molecules: Siting and segregation in silicalite zeolite. Langmuir, 16, 3910-3919.

[12] Krishna, R.; Baur, R. (2003). Modelling Issues in Zeolite Based Separation Processes. Sep. Purif. Technol. 33, 213-254

[13] D.Paschek, R.Krishna (2001),Inter-relation between self-and jump-diffusivities in zeolites, Chem. Phys. Lett. 333 278–284.

[14] R. Krishna, D. Paschek, Verification of the Maxwell–Stefan theory for tracer diffusion in zeolites, Chem. Eng. J. 85 (2002) 7–15.

[15] Skoulidas and David S. Sholl (2002). Transport b Diffusivities of CH4, CF4, He, Ne, Ar, Xe, and SF6 in Silicalite from Atomistic Simulations Anastasios I. The Journal of Physical Chemistry B 2002 106 (19), 5058-506 DOI: 10.1021/jp014279x

[17] R. Krishna,(1993)A unified approach to the modelling of intraparticle diffusion in adsorption processes,Gas Separation & Purification,Volume 7, Issue 2,,Pages 91-104,ISSN 0950-4214,https://doi.org/10.1016/0950-4214(93)85006-H.

[18] Myers, A. L., & Prausnitz, J. M. (1965). Thermodynamics of mixed-gas adsorption. AIChE Journal, 11(1), 121-127. doi:10.1002/aic.690110125

[19]Davis, M. E., & Davis, R. J. (2012). Fundamentals of chemical reaction engineering. Mineola, NY: Dover Publications.

[20] Krishna, R., Baur, R., & Van Baten, J. M. (2017). Highlighting diffusional coupling effects IN Zeolite catalyzed reactions by combining THE Maxwell–Stefan AND LANGMUIR– HINSHELWOOD FORMULATIONS. Reaction Chemistry & Engineering, 2(3), 324-336. doi:10.1039/c7re00001d

[21] BAUR, R., & KRISHNA, R. (2004). Effectiveness factor for zeolite catalysed isomerization reactions. Chemical Engineering Journal, 99(2), 105-116. doi:10.1016/j.cej.2003.09.007

[22] Krishna, R., Baur, R., & Van Baten, J. M. (2017). Highlighting diffusional coupling effects IN Zeolite catalyzed reactions by combining THE Maxwell–Stefan AND LANGMUIR– HINSHELWOOD FORMULATIONS. Reaction Chemistry & Engineering, 2(3), 324-336. doi:10.1039/c7re00001d

[23] https://youtu.be/3uvxOZkwR9w